energy&fuels

pubs.acs.org/EF
Article

Prediction of Viscosity of the Oil−Surfactant−Brine Microemulsion Phase Using Molecular Dynamics Simulations

Akash Talapatra* and Bahareh Nojabaei

Cite This: *Energy Fuels* 2024, 38, 7746−7757

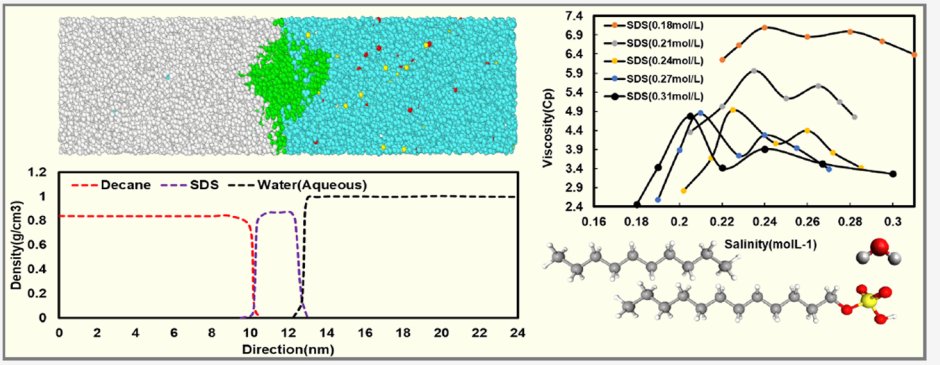

ABSTRACT: Estimation of the microemulsion dynamic viscosity under reservoir conditions is important as it is directly connected to the oil recovery predictions and optimization design. The dynamic viscosity of the microemulsion phase depends on not only the phase behavior but also the microstructure of the phase. Here, we aim to fundamentally understand and quantify the relevance of microemulsion phase viscosity to the surfactant concentration, water salinity, pressure, and temperature by conducting numerical design of experiments using molecular dynamics (MD) simulations. We use the Einstein relation, which is a reformulated Green−Kubo formula, to calculate and track the change in viscosity with the above-mentioned conditions. After our model is validated by comparing the simulated results with the available experimental data, the viscosity peaks or percolation thresholds are investigated for a specific range of salinity and surfactant concentrations. The outcome of this research results in achieving optimized rheological properties of oil−brine interfacial systems for oil recovery operations.

1. INTRODUCTION

Primary recovery of conventional oil reservoirs comprises reducing the pressure at the production well for oil to flow to the wellbore following Darcy's1,2 *Ss*. In doing so, a certain amount of oil will be left in the reservoir as residual oil.[1] To recover that amount, injecting fluid from another well can assist production by displacing the residual oil and mobilizing it.[2] Adding surfactant to the displacing fluid, typically water or brine, further enhances the oil recovery by reducing the interfacial tension (IFT) of oil and water and consequently results in an improved displacement efficiency (surfactant flooding).[3] This addition of surfactant to the oil/brine system introduces additional complexities to the multicomponent multiphase fluids at the reservoir condition, as it leads to an altered phase behavior and one (or two) additional liquid phase(s). The newly formed phase is called the microemulsion phase and it is thermodynamically stable.[4] Surfactant molecules have a dual structure, with a hydrophilic head and a lipophilic tail, and show a strong affinity to aggregate on the interface between oil and water, therefore reducing surface forces at the oil/brine interface and consequently decreasing the IFT. Depending on the surfactant type (ionic vs nonionic), mass fraction of surfactant, temperature, pressure, brine salinity, and type of oil, the configuration of surfactant aggregates can be different.[3,5] Micelles are aggregates of surfactant molecules dispersed in a liquid colloid. When oil and water are mixed, micelles can form, and the configuration of these micelles depends on various conditions.[6]

Among the reservoir fluid properties, viscosity is directly related to phase mobility and therefore is a critical parameter in recovery calculations.[7] To this end, microemulsion viscosity predictions and quantification, along with the viscosity of the oil and water phases, are required for enhanced oil recovery (EOR) designs. The microemulsion viscosity and how it varies with

Received: December 9, 2023
Revised: April 2, 2024
Accepted: April 9, 2024
Published: April 18, 2024

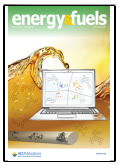

salinity, pressure, temperature, and other factors have been experimentally characterized by several researchers, and a few experimental correlations have also been developed for certain conditions.[8] Considering that the practical reservoir condition is very dynamic during recovery, reservoir engineers need to accurately estimate and calculate the viscosity and other important fluid properties of present phases in the reservoir at various pressures, temperatures, brine salinity, oil concentration and composition, and surfactant mass fraction. To do so, several phase behavior models have been developed, including the broadly used Hand's empirical model,[9] and other more advanced phase behavior models, such as the one proposed by Acosta et al.,[10] which is based on the surfactant affinity difference toward oil or water, or hydrophilic−lipophilic difference (HLD), and correlating solubility to the micellar characteristic length. Ghosh and Johns[11,12] and later Khorsandi and Johns[13] further extended these models and made them work for all Winsor's multiphase types. Note that all of these phase behavior models only provide information about the phase compositions, number of phases, and IFT.

Viscosity is not only a function of macroscopic thermodynamic properties of the microemulsion phase but also changes with the microemulsion microstructure. The viscosity of the microemulsion phase was calculated and reported to have an M shape function for the changes in viscosity with salinity. Typically, by increasing salinity, viscosity increases, and after reaching a maximum, it drops to a local minimum, increases again, and decreases as it approaches the oil viscosity, although a few research studies reported zero local minimum.[14,15] It is still not clear how the viscosity peaks are exactly correlated with multiple factors, such as salinity, surfactant concentration, pressure, and temperature. Multiple researchers proposed different models to predict the surfactant/oil/brine viscosity, but they could not predict the M shape profile or viscosity peaks.[8] The same is true with the viscosity models of the widely used simulation tools, such as Computer Modeling Group (CMG)[16] by the oil industry. The only microemulsion viscosity model that predicts the M shape and magnitude of viscosity reasonably accurately is the one developed by Khodaparast and Johns.[17] They developed an equation of state (EoS) phase behavior model known as the net-average-curvature (NAC) model based on the hydrophilic−lipophilic difference (HLD-NAC). However, that model did not capture the location of low-viscosity points. Therefore, they tuned the viscosity peaks by using the experimental data rather than predicting them.

Scriven[18] was the first to come up with the theory that the microemulsion phase configuration can have a bicontinuous structure and be represented by interpenetrating subdomains of water and oil, each of them physically continuous. Khodaparast and Johns[17] explained the viscosity changes with salinity by analyzing the microemulsion microstructure changes in the following order: water continuous with oil micelles, water bicontinuous with partial oil continuous, water and oil bicontinuous, oil bicontinuous with partial water continuous, and oil continuous with water micelles. Their rationale was that micelles act as solid spheres against the flow and consequently increase viscosity compared to only water or only oil phase, while the bridge-like connections in the bicontinuous structure decrease the microemulsion viscosity. Peyrelasse et al.[19] called the onset of bicontinuity, which accurately correlates to the viscosity peaks as percolation thresholds.

As the next step, researchers searched for a connection between the microstructural changes mentioned above and the percolation thresholds with the microemulsion phase behavior. Lipgens et al.[20] used small-angle neutron scattering to study the water/c-hexane/Igepal microemulsion percolation transition for multiple temperatures and concluded that changing temperature shifts both percolation thresholds, however, it does not broaden the percolation region. Laurati et al.[21] used small-angle neutron scattering to analyze the transition of water in oil micelles to droplet clusters and referred to these phenomena as "dynamic fusion"; however, no information was provided about any potential correlation between the percolation threshold and temperature. Jeirani et al.[22] applied the design of experiments to predict the percolation thresholds by using the dynamic viscosity data. Like the previous research studies that aimed at quantifying the percolation threshold, this work was also limited to one variable parameter, which was the water volume fraction.

Although multiple research studies aimed to analyze the microemulsion phase microstructure and viscosity,[21,22] there are still quite a few unanswered fundamental questions, yet with practical implications, about the design parameters, and the viscosity of the water/oil/surfactant system. Previous researchers worked on the oil−surfactant−brine viscosity measurement, focusing on type I or II regions;[8,23] however, in the current viscosity models, the percolation thresholds are adjusted and tuned to the limited available experimental results.[17] It is still unknown how percolation thresholds differ for different surfactant concentrations. In this study, we computationally calculate the viscosity of the brine−surfactant−oil microemulsion phase for different salinities, surfactant concentrations, pressures, and temperatures. The goal of this research is to specify the factors that influence the percolation threshold and consequently predict the viscosity peaks of the microemulsion phase. Different mixtures of the oil−surfactant−brine system are modeled by using a computational approach in a range of practical pressures, temperatures, surfactant concentrations, and salinity. Therefore, this study offers an understanding of the transition in microemulsion phase viscosity for a better prediction accuracy later.

2. METHODOLOGY

2.1. Molecular Dynamics Simulation Method. The fundamental theory of molecular dynamics (MD) simulations is to observe the dynamic trajectory of an atomic system and analyze the atomic interactions among the respective atoms by solving Newton's equation of motion.[24] Here, in this paper, the molecular scale study is performed on the oil−water interfacial system using a Large-scale Atomic/Molecular Massively Parallel Simulator (LAMMPS) software package.[25] The microemulsion systems are made up of decane, sodium dodecyl sulfate (SDS—an anionic surfactant), and water. The Na^+ and Cl^- ions are dissolved in the water phase, and decane represents the oil component. The simulation box contains a single interface composed of all components, with the molecular structures depicted in Figure 1. The interfacial properties are studied at various temperatures, pressures, concentrations of SDS, and salinity.

The atomic interactions in the oil and SDS molecules are described by the OPLS-AA potential, while the SPC/E is used to model water molecules, which accounts for the internal vibrations and bond flexibility. These force fields have undergone extensive testing and have been successfully utilized in prior simulation works.[26,27] All of the force field parameters for OPLS-AA and SPC/E are collected from the Automated Topology Builder (ATB) and Repository.[28] The Lorentz−

https://doi.org/10.1021/acs.energyfuels.3c04902
Energy Fuels 2024, 38, 7746−7757

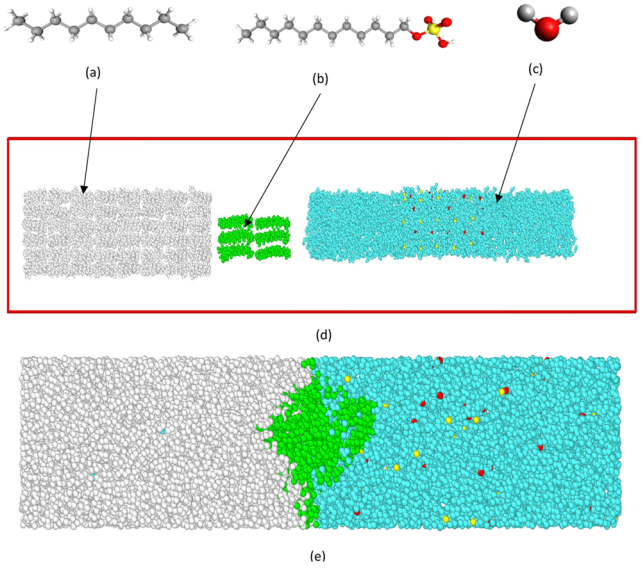

Figure 1. Simulation system and structures. (a) Decane, (b) sodium dodecyl sulfate (SDS), (c) water, (d) initial system (yellow: Na^- and red: Cl^-), and (e) the interfacial system after equilibration.

Berthelot rule[29] is used to obtain the potential parameters between crossing atoms. The harmonic potential is used for bonded interactions, such as bond stretching, angle bending, and dihedral angle torsion in intermolecular interactions. For nonbonded interactions, the short-range van der Waals (Lennard-Jones interaction) plus the long-range Coulombic interactions is applied. The Lennard-Jones potential[30] and its parameters (ε_{ij} and σ_{ij}) between different atom types are obtained using geometric combining rules as shown in eqs 1, 2, and 3.

$$V_{lj} = 4\varepsilon\left[\left(\frac{\sigma}{r}\right)^{12} - \left(\frac{\sigma}{r}\right)^{6}\right] \quad (1)$$

$$\varepsilon_{ij} = \sqrt{\varepsilon_{ii}\varepsilon_{jj}} \quad (2)$$

$$\sigma_{ij} = \sqrt{\sigma_{ii}\sigma_{jj}} \quad (3)$$

In the simulations, all of the atoms are free to adjust their positions to attain equilibrium structures. Moltemplate is used to generate the simulation model for the oil−surfactant−water interfacial system. It is a cross-platform text-based molecular builder particularly made for LAMMPS. The initial configuration and molecule numbers of all of the components are given in Table 1. Different reservoir and thermodynamic conditions are considered for this study. The range of pressures, temperatures, SDS concentrations, and salinities used in our simulation are listed in Table 2. Note that all of the possible combinations of temperatures, pressures, SDS concentrations, and salinities are not considered here. Pressure and temperature are fixed at 100 bar and 300 K, respectively, for investigating the effect of SDS concentration and salinity on viscosity. Initially, the energy of the system is minimized using the steepest descent minimization method. Then, the number of molecules (N), pressure (P), and temperature (T) are maintained constant during the next stage of simulation. This system is equilibrated using an NPT ensemble for 4 ns with a time step of 2 fs. Temperature (300 K) and pressure (100 bar) are controlled by a Nose−Hoover thermostat and Parrinello−Rahman barostat, respectively. The coupling constants for temperature and pressure are 1 and 10 ps. There was some vacuum space inside the box (Figure 1d), which was removed during the equilibration period (Figure 1e). The temperature and total energy of the system are properly maintained constant (shown in Figure 2). After 4 ns, the NPT ensemble changes to the NVT for further production run on the equilibrated system up to 8 ns.

Table 1. Initial Configuration and Molecule Numbers of All of the Components

material type	dimension (Å^3)	potential	number of atoms
decane	240 × 50 × 50	OPLS-AA	9216
SDS		OPLS-AA	1032 (0.21 mol L^{-1})
brine		SPC/E	9114 (salinity of 0.18 mol L^{-1})

Table 2. Simulation Conditions[a]

SDS concentration (mol L^{-1})	0.11	0.15	0.18	0.21	0.24	0.27	0.31
salinity (mol L^{-1})	0.11	0.13	0.18	0.21	0.25	0.3	0.35
temperature (K)	300	330	360	390	420	450	
pressure (bar)	100	130	160	190	230	260	

[a]For each concentration of SDS and salinity, a series of simulations are conducted under varying temperature and pressure conditions.

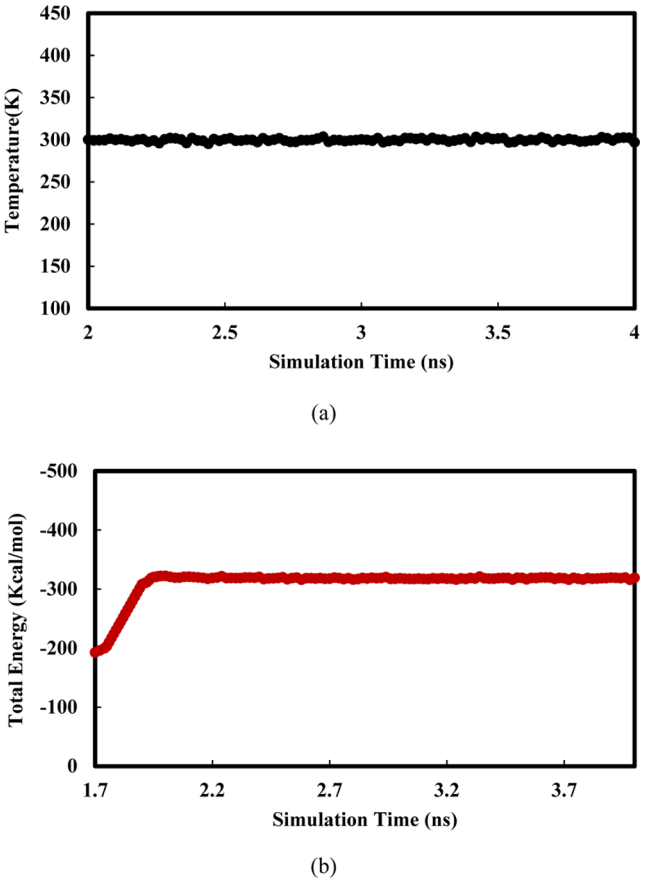

Figure 2. Variations in the temperature and energy curves of dynamic simulation for the initial system at the equilibration state up to 4 ns. (a) Temperature and (b) total energy.

https://doi.org/10.1021/acs.energyfuels.3c04902
Energy Fuels 2024, 38, 7746−7757

The Boltzmann function is used to set an initial velocity distribution throughout the system according to the respective temperature. The periodic boundary conditions are used in all directions of the simulation box. For the equilibration stage, atom trajectories are recorded every 0.1 ns, then every 0.5 ns for the production stage, to capture the morphological dynamics of the microemulsion phase. The LINCS[31] algorithm is used to constrain all bond and angle algorithms. Besides, due to the significant electrostatic interactions between ions and water molecules, the particle−particle−particle−mesh (PPPM) method is used with a 1.2 nm pairwise cutoff distance (for both electrostatic and van der Waals interactions) to compute the long-range Coulombic interactions. OVITO[32] software is used to visualize the trajectories of the simulation.

2.2. Radial Distribution Functions (RDFs). The radial distribution function (RDF), denoted as $g(r)$, represents the density variation near specific particles. It is commonly used to describe the local microstructure of fluids. The pairwise interaction and coordination number between groups of nearest neighbor atoms are calculated using that function in a bonded simulated system. It represents the likelihood of finding a particle at a certain distance (r) from a reference atom in the molecule.[33,34] Specifically, it determines the distribution of particles surrounding a central particle. The formula for RDF[24] is given by

$$g_{ij}(r) = \frac{\langle \Delta N_{ij} \rangle}{\rho_j V_{ij}} \tag{4}$$

where i represents the central atom, j represents the atom around the central atom, ΔN_{ij} denotes the number of atoms in the layer, and ρ_j is the average number density of atom j. As the distance increases, $g(r)$ approaches one, indicating that the number density of atom j is homogeneous and equal to the average number density. In this context, we focus on the $g(r)$ of S−Na, S−H, S−O, and S-decane to understand the interfacial properties of the microemulsion phase.

2.3. IFT Calculation. Here, in this study, the interfacial tension (IFT)[35] is calculated computationally by calculating the pressure tensors throughout the interface (toward the x direction) during the NVT simulation. The expression for IFT is given below:

$$\gamma = \left(\left(-\left(\frac{x_{hi} - x_{ho}}{2} \right) \right) \left(\frac{p_{zz} + p_{yy}}{2} \right) - p_{xx} \right) 0.0101325 \tag{5}$$

where γ is the interfacial tension (mN/m), x_{hi} and x_{ho} are the dimensions in the x direction; p_{xx}, p_{yy}, and p_{zz} are the diagonal components of pressure tensors in the respected system, and 0.0101325 is the conversion factor.

2.4. Phase Viscosity Calculation. A widely used, Green−Kubo (GK) formula considers the statistical mechanical principles to predict the transport property (viscosity) of a liquid−liquid interfacial system.[36] Hence, the MD simulation generates data on the mechanical properties (velocity, pressure, and heat flux) of the systems being simulated based on the underlying principles of statistical mechanics.[25] The fluctuations of those mechanical properties are considered to estimate the viscosity using GK formulation.[36,37] This formulation demonstrated the coefficients that can be expressed as integrals of equilibrium time autocorrelation functions (eq 6)

$$\mu = \frac{V}{k_B T} \int_0^\infty \{ \tau_{\alpha\beta}(t_0) \tau_{\alpha\beta}(t) \} dt \tag{6}$$

where μ is the viscosity (cP), k_B denotes Boltzmann constant, V represents the volume of the system, T is the temperature (K), and $\tau_{\alpha\beta}$ represents off-diagonal components of the stress tensor at the time, t. The component of the stress tensor (for N particles) is calculated by the following formula and Newton's equation as follows:

$$\tau_{\alpha\beta} V = \sum_{i=1}^{N} m_i v_{ix} v_{iy} + \sum_{i=1}^{N} r_{ix} f_{iy} \tag{7}$$

$$m_i r_i = F_i(r_1, \ldots\ldots\ldots, r_1) \tag{8}$$

where v is the velocity, m is the mass, r_i denotes the radius vector, and F_i is a force acting on the ith particle.

The calculation of viscosity using the GK formula considers the integration of correlation functions over a long period interval (0, ∞). This formula requires the calculation of time and velocity correlation functions over time, as well as storing the trajectories of all particles, which increases the simulation time and cost for many molecules. Then, an equivalent expression of the GK formula derived by Helfand[38] considering the Einstein-type relations is established as follows:

$$\mu = \lim_{N,V,t\to\infty} \frac{V}{2k_B T} \frac{d}{dt} \langle (G(t) - G(0))^2 \rangle \tag{9}$$

where $G(t) = \frac{1}{V} \sum_{i=1}^{N} r_i(t) P_i(t)$ and P_i is the momentum of particles for ith particle. The above formula is again revised[38] to overcome the discontinuity caused by the periodic boundary conditions and expressed as follows:

$$\mu = \lim_{N,V,t\to\infty} \frac{V}{2k_B T} \frac{d}{dt} \left\langle \left(\int_{t_o}^{t_o+1} P_i(t) dt \right)^2 \right\rangle \tag{10}$$

This Einstein relation (reformulation of the GK relation) for viscosity calculation considers the kinetic theory of Brownian motion (based on the diffusion coefficient) and is much simpler than the GK formula. Besides, this relation is much more valid and accurate for the system with many-body interactions and is found to be less computationally time-consuming and expensive.

2.5. Density Calculation. The density profiles for this current decane/SDS/brine interfacial system along the direction normal to the x-axis are shown in Figure 3. This configuration is shown after the equilibration of the system by using the NPT ensemble. The oil and brine components are uniformly

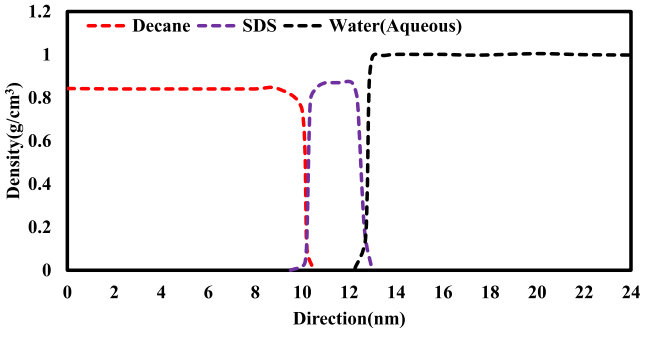

Figure 3. Simulated and equilibrated density profiles of the oil, surfactant, and brine phases at 300 K and 100 bar.

https://doi.org/10.1021/acs.energyfuels.3c04902
Energy Fuels 2024, 38, 7746−7757

distributed throughout the x direction with densities of 0.84 and 1.01 g/cm^3, respectively, including surfactant molecules in the middle phase (0.87 g/cm^3). The density calculations are done at a temperature of 300 K and a pressure of 100 bar. The densities[39] of the components are calculated using eq 11:

$$\rho = \frac{NM}{\langle V \rangle} \tag{11}$$

where N is the number of molecules, M is the molecular weight, V is the total volume of the components, and $\langle \cdot \rangle$ denotes the ensemble average. The calculated densities for oil and water components are in line with the actual reservoir conditions.[40] From the density profile, the interface thickness is found around 3 nm with an abrupt transition of the phases, where surfactant molecules are present. The accompanying change in the microemulsion density as a function of salinity is shown in Figure 4. The figure shows that the microemulsion density is

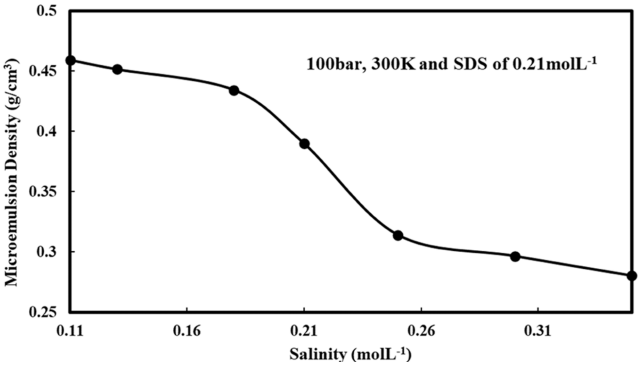

Figure 4. Microemulsion density vs salinity at the interface.

0.46 g/cm^3 for the salinity of 0.18 mol L^{-1}, which is decreased by 38.90% for increasing the salinity by 2.5%. The reason is that the ratio of water to oil is increased for increasing salinity. This can be illustrated by the previous studies considering the relative volume[4] of the microemulsion phase using eq 12:

$$V_o/V = (\rho - \rho_{water})/(\rho_{oil} - \rho_{water}) \tag{12}$$

where V_o/V is the volume fraction of oil. The higher the volume fraction, the lower the microemulsion density. This is beneficial for surfactant flooding in enhanced oil recovery since it can solubilize and mobilize more oil components in the interface.[4]

3. RESULTS AND DISCUSSION

3.1. Atomic Interactions among the Microemulsion System. In this decane−SDS−brine interfacial system at 300 K and 100 bar, the water molecules and counterions are found closest to the SDS head groups (SO_3^{2-}). From Figure 5, it can be shown that the first peaks in the RDF of S−H, S−Na$^+$, and S−O are near 1, 1.08, and 1.25 nm, respectively. The results are consistent with previous simulations.[34,35] The presence of water molecules near the SDS head groups is possibly due to hydrogen bonding. S-decane is farther from the SDS head groups. The peak in the RDF for S-decane is near 1.45 nm since the SDS headgroup has weaker interactions with decane with a magnitude of 5.19. The reason is that the alkyl tails of SDS strongly interact with the decane molecules. The RDF between oil molecules and S gives a quantitative evaluation of the effect of surfactants on the monolayers at the interface. The changing of salt ions does not affect the chemical potential of the oil

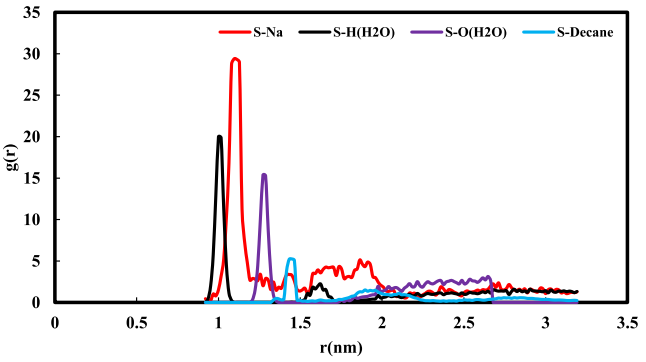

Figure 5. RDFs of the decane−SDS−brine microemulsion system.

component. Regarding the applied force fields of the molecules in this study, the molecules are interacting similarly close to the previous experimental works.[35]

3.2. Validation—Effect of SDS Concentrations on IFT. Validation is important to ensure that the model accurately represents the actual reservoir conditions. The IFT results of our work on the decane/brine interfacial system in the presence of SDS as well as the accuracy of the outputs are validated with the experimental results (considering a 10% percentage error bars in the experimental results) from Rehfeld[41] for the same conditions (300 K and 100 bar). The IFT results at a salinity of 0.18 mol L^{-1} under different SDS concentrations (0.11−0.31 mol L^{-1}) are shown in Figure 6. As can be observed, our work's IFT values are

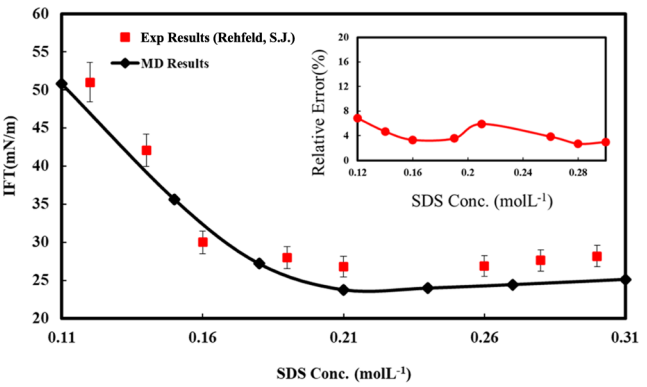

Figure 6. Effect of SDS concentration on microemulsion IFT (at 300 K, 100 bar, and a salinity of 0.18 mol L^{-1}).

close to the results of past work. With the increase of SDS concentrations, the equilibrium IFT gradually goes down. For the increasing concentration up to 0.21 mol L^{-1}, the IFT reduction (from 50.7684 to 23.7895 mN/m) is quite sharp due to the adsorption of SDS in the interface. While the concentration is increasing toward the critical micelle concentration (CMC), the negatively charged hydrophilic headgroup of SDS (SO_4^-) typically resides in the aqueous phase (brine) and the positively charged hydrophobic 12-carbon hydrocarbon chain resides in the oil phase (decane). This orientation allows SDS to mediate between the two phases by forming strong interactions with both, resulting in a decrease in IFT.[42] But, after reaching the concentration of 0.21 mol L^{-1}, IFT values remained nearly horizontal for the increasing SDS concentration up to 0.31 mol L^{-1}. Since the minimum IFT value is found at 0.21 mol L^{-1} (23.7895 mN/m), this is the optimum or critical micelle concentration (CMC) of the SDS for our

https://doi.org/10.1021/acs.energyfuels.3c04902
Energy Fuels 2024, 38, 7746−7757

model. At the CMC, the cluster of micelles is shielded from the aqueous phase, leading to the minimum value of the IFT. When the concentration is above 0.21 to 0.31 mol L^{-1}, the adsorption of surfactant molecules gets saturated and stops adsorbing more SDS molecules. This consequently keeps the IFT values near constant for increasing surfactant concentrations.

The size and number of micelles increase for the increasing SDS concentration beyond CMC, but the growing formation of micelles is not able to significantly reduce the IFT further.[43] The excess of surfactant molecules is present in the bulk phase, and they do not contribute significantly to the interfacial properties of the system. The aggregation of the surfactant molecules at higher concentrations causes the formation of micelles in the shape of spherical or cylindrical.[44] The surfactant molecules still could maintain their orientation in the microemulsion phase. However, the IFT reduction in microemulsion works as a piston-like displacement (of the microemulsion phase by water and oil by the microemulsion phase) for enhancing oil recovery. In addition, the current results of IFT reduction indicate that beyond the CMC, surfactant tends to populate the decane–brine interface, which in turn increases the capillary number and decreases the residual saturation.[45]

3.3. Validation—Effect of SDS Concentrations on Microemulsion Viscosity. The oil continuous phase transforms into a bicontinuous phase system (with surfactant and brine) and ultimately into a brine continuous system. These three phases have distinct structural organizations that result in significant changes in phase viscosity caused by the alteration of surfactant and salinity concentrations.[44,46−51] For microemulsion viscosity calculation and validation in the decane–brine interface, similar conditions are used as those used for IFT calculation. The shear rate is considered around 5.6 s^{-1} for the calculations of viscosity. Particularly for microemulsion phases, the viscosity is almost insignificant to the shear rate.[8] First, the viscosity values for a NaCl concentration of 0.18 mol L^{-1} (at 300 K) are calculated, and later, these results are validated with the previous work (considering a 10% percentage error bar in the experimental results) for the same conditions done by Nespolo et al.[52] at 300 K. Based on the obtained results (300 K and 100 bar), Figure 7 is plotted, and we have found that the current results agree with the previous work for the SDS and salinity conditions.

The microemulsion phase viscosity is affected by the SDS concentrations. According to Figure 7, the microemulsion viscosity curve reaches 5.82 cP for the SDS concentration up to 0.18 mol L^{-1}, followed by decreasing sharply to 2.35 cP for the increasing concentration of 0.24 mol L^{-1}. The viscosity values remain almost unchanged when the SDS concentrations further increase to 0.31 mol L^{-1}. After the threshold concentration of SDS (0.18 mol L^{-1}), the viscosity is independent of the surfactant concentrations. SDS molecules form small and spherical micelles at low concentrations, but as the concentration increases, the micelles grow and become elongated or rod-like and ultimately become entangled. This entanglement increases the viscosity of the microemulsion phase by hindering the movement of micelles.[53,54] The micelles become more compact and tightly packed for the concentration of SDS from 0.18 to 0.24 mol L^{-1}. This change in micelle structure, from a more dispersed state to a more compact state, influences the microemulsion's flow behavior.[55,56] This phenomenon reduces the available space for the movement of micelles and leads to a decrease in the phase viscosity.

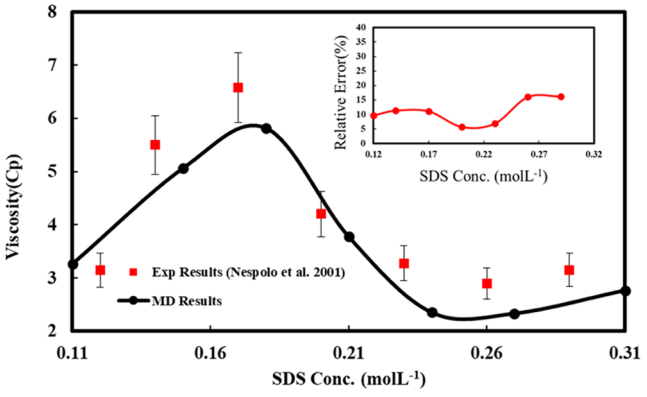

Figure 7. Effect of SDS concentrations on microemulsion viscosity (at 300 K, 100 bar, and a salinity of 0.18 mol L^{-1}).

However, the interfacial system moves into the equilibrium phase when the micelle formation reaches a state of saturation. Further additions of SDS molecules do not lead to any significant change in micelle structure or intermolecular interactions. Due to this maximum packing density and stabilization of micelles, the microemulsion phase results in little change in viscosity. The microemulsion phase viscosity is influenced by hydrophilic and hydrophobic interactions of the surfactant molecules.[17] The addition of salinity affects this interaction by changing the solubility of the surfactant in the aqueous phase.[49] In Figure 8, the microemulsion viscosity

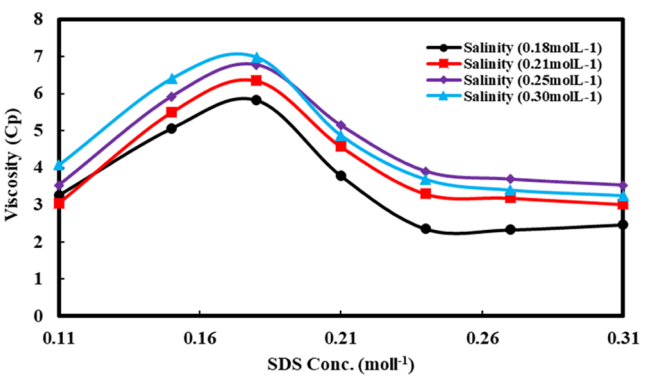

Figure 8. Effect of SDS concentrations on microemulsion viscosity at different salt concentrations (at 300 K and 100 bar).

changes over SDS concentrations under different salinity conditions are shown. The changing trends in viscosity at 300 K and 100 bar are similar for other salinity conditions (0.21–0.30 mol L^{-1}).

3.4. Effect of Simulation Time. A reasonable and justified simulation time is a crucial factor in increasing the accuracy and reducing computational costs. Figure 9 shows the changes in viscosity values over a simulation time considering the equilibration of the system. Here, the oil/water interfacial model has run with different SDS concentrations (from 0.11–0.31 mol L^{-1}) for the simulation time (0–8 ns) to investigate the effect of time on microemulsion viscosity. All of the computational processes are done here at the start of NVT integration (production phase). The viscosity curves go through the same trend of changes for different SDS concentrations. Initially, for all cases, the system reaches the minimum microemulsion viscosity, then it remains constant for a prolonged simulation time for the SDS concentrations. For example, at the early stage

https://doi.org/10.1021/acs.energyfuels.3c04902
Energy Fuels 2024, 38, 7746−7757

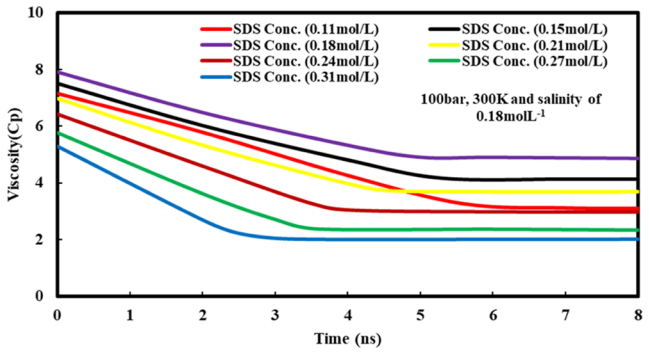

Figure 9. Changes in microemulsion viscosity over the simulation time for different SDS concentrations at 300 K, 100 bar, and a salinity of 0.18 mol L^{-1}.

of the simulation (for SDS of 0.11 mol L^{-1}), the viscosity is found around 7.14 cP, followed by a minimum value of 3.26 cP at 5.6 ns. Then, this value remains nearly the same for continuing the simulation (up to 8 ns). The noticeable thing is that this colloidal dispersion system achieves the minimum point of viscosity earlier for increasing SDS concentrations due to the faster formation of sphere-like droplets. The higher SDS concentration usually initiates the self-microemulsion process[57] system faster for having a higher oil–water ratio in the microemulsion phase. This can be understood by studying the diameter and surface area of the formed droplets from previous studies.[58] The diameter (D) and surface area (A) of those droplets[58] can be calculated using eqs 13 and 14:

$$D = \sqrt[3]{\frac{6 \times \rho \times N_w}{\pi}} \tag{13}$$

$$A = \pi D^2 \tag{14}$$

where ρ is the density of the water and N_w is the number of water molecules. The changes in microemulsion droplets over time can be divided into two parts. The first part is for indicating the evolution of the microemulsion droplet until it reaches the minimum viscosity value. On the contrary, the second part indicates the stabilization of those droplets after the equilibrium state.[59] From Figure 9, the viscosity remains higher initially due to the small size and nonuniform distribution of the microemulsion droplets throughout the interface. The free water molecules not fully coated by SDS head groups (SO_3^{2-}) diffused in the oil phase, contributing to the increasing droplet sizes according to the droplet coalescence theory. With increasing simulation time, the droplet size increases and its distribution becomes uniform. The required time for droplet size evolution decreases with an increasing SDS concentration because of the faster coalescence of droplets. The velocity distribution and morphology of the interface are not necessarily affected by the speed of the faster droplet formation.[58,59] It is worth noting that the interface becomes narrower with time also.[57] After reaching stabilization of the droplet formation in the equilibrium state, a longer simulation time cannot change the energy state and phase separation phenomena of the droplets. In terms of surface area, the longer simulation time lowers the surface area of the microemulsion droplets, which is favorable for the stabilization of the system. Again, this can be illustrated by a recent study done by Li et al.,[60] which observed that initially, the surfactant molecules dispersed in the aqueous water and slightly bent down, which creates a repulsion between the head groups. The head–head repulsion (α_{HH}) caused by SO_3^{2-} groups showed a value of 22. As the simulation time passed, small droplets formed and eventually started merging to become stable droplets (α_{HH} reduced to 14).[60] As a result, the end-to-end distance between the hydrophilic SO_3^{2-} group and the hydrophobic long-chain alkyl group of the surfactant molecules increases caused by the Na^+ concentrations from aqueous water. This reduced the electrostatic repulsion and allowed more extended surfactant molecules at the oil–water interface. This phenomenon continues until the system reaches the equilibrium state; after that, this repulsion neutralizes for the increasing adsorption of surfactant molecules in the oil–water interface. To further validate these phenomena, the interfacial emulsification rate (R)[61] of this system is calculated using the following expression:

$$R = \frac{\int_{x_1}^{x_2} \rho_{SDS}(x)\mathrm{d}x}{\int_{x_1}^{x_2} \rho_{sys}(x)\mathrm{d}x} \tag{15}$$

where $\rho_{SDS}(x)$ is the density of SDS (g/cm^3) and $\rho_{sys}(x)$ is the density of all components in the x direction, x_1 and x_2 define the positions, where the SDS start to appear at the interface and completely disappear, respectively. R is a unitless parameter. By integrating the density distribution along the x direction, the changes in interfacial emulsification rate are calculated using eq 15 and shown in Figure 10 over a prolonged simulation time.

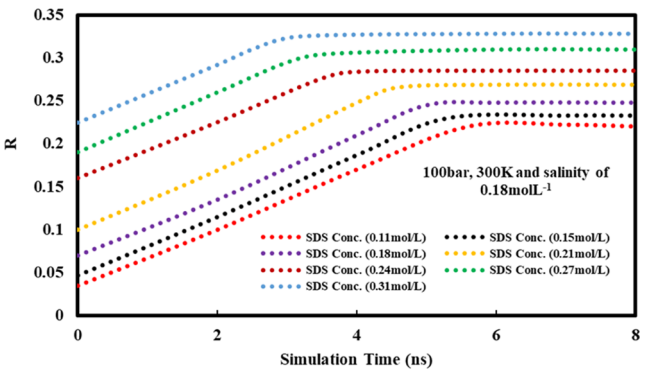

Figure 10. Effect of simulation time on the emulsification rate for different SDS concentrations at 300 K, 100 bar, and a salinity of 0.18 mol L^{-1}.

From Figure 10, the emulsification rate, R, increases linearly first and then plateaus, indicating that the aqueous and oil phases become more miscible as time increases. For example, the R-value is found at 0.17 (SDS of 0.11 mol L^{-1}) at nearly 5.5 ns and then plateaus up to 8 ns. The reason is that when more surfactants are added, they begin to cover the interface more and more. This is also known as interfacial coverage.[61] After reaching the maximum interfacial coverage, the microemulsion has achieved a stable state, where the uniform distribution of aqueous and oil components is not changed by adding more surfactants.[61] In addition, the emulsification rate is found to be higher for higher SDS concentrations. The peak of the emulsification rate (0.33) is observed at 3.2 ns (for SDS of 0.30 mol L^{-1}), whereas it takes approximately 5.3 ns for SDS of 0.15 mol L^{-1}. This is a result of an enhanced emulsification mechanism. As the number of SDS molecules increases, the value of the hydrophilic–lipophilic balance also increases, indicating a greater affinity for the aqueous phase. This rapidly

https://doi.org/10.1021/acs.energyfuels.3c04902
Energy Fuels 2024, 38, 7746–7757

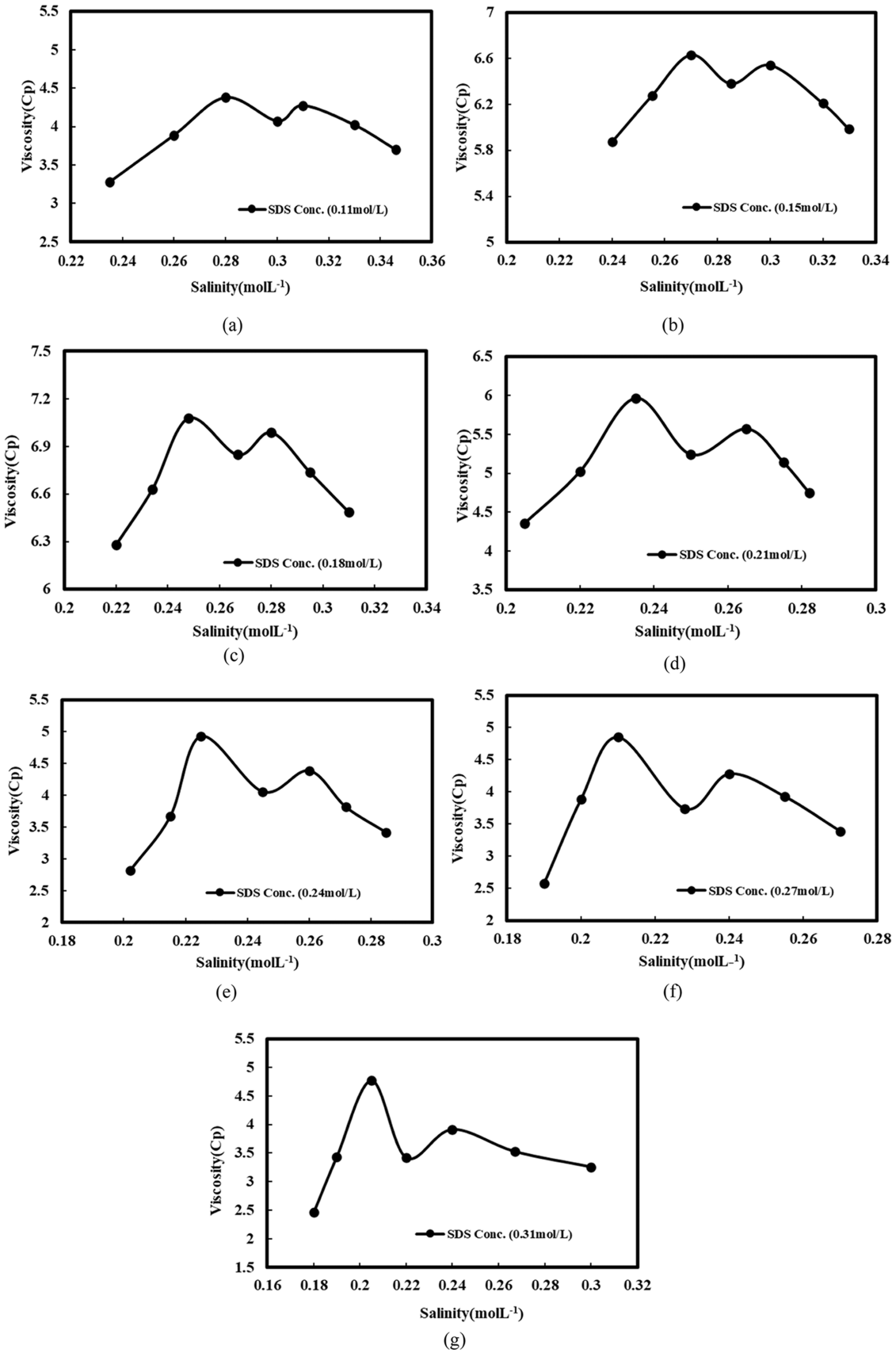

Figure 11. Effect of salinity on microemulsion viscosity for different SDS concentrations at 300 K and 100 bar: (a) 0.11 mol L^{-1}, (b) 0.15 mol L^{-1}, (c) 0.18 mol L^{-1}, (d) 0.21 mol L^{-1}, (e) 0.24 mol L^{-1}, (f) 0.27 mol L^{-1}, and (g) 0.3 mol L^{-1}.

https://doi.org/10.1021/acs.energyfuels.3c04902
Energy Fuels 2024, 38, 7746−7757

increases the dispersion and molecular weight of the droplets in the interface with the simulation time.

3.5. Effect of Salinity Concentrations on Microemulsion Viscosity. The microemulsion viscosity exhibits varying behavior for different SDS concentrations at 300 K and 100 bar across different salinity levels. The viscosity results are listed in Figure 11. The obtained microemulsion viscosity curve is like a unique "M" shape and shows two peaks (meaning that it increases to maximum values twice) as salinity increases due to the phase changes from oil to brine. This phase transition occurs from a lamellar structure (oil domain separated by a bilayer of surfactant molecules) to a bicontinuous structure (oil and water domains are interconnected) and again to a lamellar structure (brine domain separated by a bilayer of surfactant molecules).[62] Usually, for Winsor microemulsion types I and II (typically 2 phases), only one maximum exists since the microemulsion phase is either oil-rich or water-rich. But for Winsor type III (of 3 phases), the microemulsion phase forms in the middle with higher surfactant molecules.[7] When the salinity is high enough for the three phases to coexist, the microemulsion phase exhibits a shear-thinning behavior. As salinity approaches the lower limit, the microemulsion's viscosity becomes extremely high, and its shear-thinning behavior becomes more pronounced. Again, both the viscosity and its shear-thinning behavior decrease as salinity increases toward the upper limit.[8] However, when the salinity increases subsequently, the ratio of oil to water also remains higher in the middle phase and microemulsion viscosity curves experience two deeper peaks. Besides, the first peak gets even sharper than the second one. The reason is that the microemulsion phase is merely intense near the boundaries. This case is also proved by performing the light scattering experiments in past works.[62] The growth of surfactant molecules in the microemulsion phase initiates the first peak to shift at lower salinities and the second peak to higher salinities, which deepens the valley between the two peaks (Figure 11). For instance, according to Figure 11a,g, the two peaks are observed for the SDS concentration of 0.11 mol L^{-1} at the salinity values of 0.28 mol L^{-1} (4.379 cP) and 0.31 mol L^{-1} (4.275 cP), whereas the peak values are found at the salinity values of 0.21 mol L^{-1} (4.773 cP) and 0.24 mol L^{-1} (3.916 cP), respectively, for the SDS concentration of 0.31 mol L^{-1}. This is due to the phase separation at higher concentrations of SDS for increasing salinity.[17] When the salinity and SDS concentrations increase, the whole system moves to the middle phase (Winsor type III) much faster than at lower concentrations. This is achieved by compressing the diffusive double-electronic layer of charged particles in water and altering the ionization balance state of the ionic surfactant.[52] The salt ions enter the interface membrane and adjust the hydrophile and lipophile deviation (HLD) value of the SDS by charging the interface membrane. Currently, some micelles change shape from spheres to hemispheres or ovals. The interface membrane begins to elongate and gradually becomes more lipophilic. This causes the oil and water phases to agglomerate and form a bicontinuous network earlier. With increasing salinity, the HLD remains at an equilibrium state, however, the alignment of the micelles is more packed, and the phase becomes more stable.[46]

3.6. Effect of Temperature and Pressure. Temperature and pressure have a significant impact on the microemulsion viscosity since they can change the structure and formation of the surfactant molecules.[63,64] Figure 12 shows the impact of increasing temperature on the variation in microemulsion viscosity for increasing salinity (at 100 bar and SDS of 0.21 mol L^{-1}). As the temperature increases from 300 to 450 K, the viscosity decreases by 23.47% for a salinity of 0.11 mol L^{-1} and by 26.69% for a salinity of 0.35 mol L^{-1}. For all salinity levels, the temperature increases consistently. The middle phase viscosity experiences a significant reduction upon the release of excess oil until reaching a specific temperature, after which it remains constant. The reason is that when a specific salinity concentration goes to an optimum salinity during the increasing temperature, then the microemulsion phase has significant stability at high temperatures.[23] Increasing the temperature beyond that causes a change in the microstructure of the microemulsion by expelling oil and water into two separate phases.[23,65] This can be interpreted by a change in spontaneous curvature (C_o) value, which depends on the interrelationship of the geometrical alkylic chain and SO_4^- of the surfactant. This value decreases with increasing temperature since it is interrelated with the hydration number of the SO_4^- groups, and the hydration number decreases at high temperatures.[51,63] The microemulsion phase's temperature dependency can be attributed to the interplay between Arrhenius behavior and micellar aggregation. As the temperature increases, thermal energy causes the hydrogen bonds to weaken, resulting in micellar aggregation and interchain association. Consequently, this causes surfactant heads to become less soluble in water and slightly can change the viscosity values in the microemulsion phase at higher temperatures.[66]

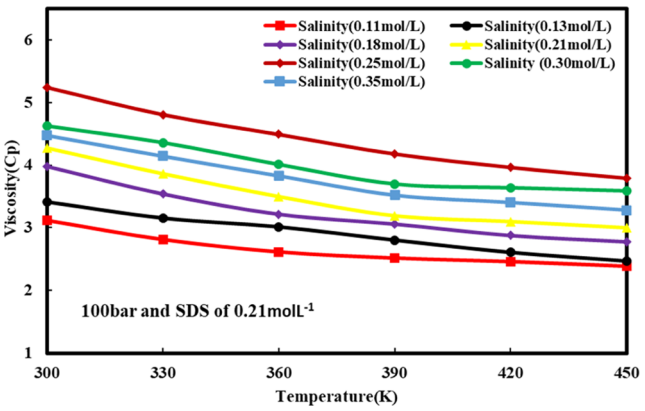

Figure 12. Temperature dependence of oil−water microemulsion viscosity at different salinities (100 bar and SDS of 0.21 mol L^{-1}).

Increasing pressure on a microemulsion results in a phase transition, a decrease in the optimum solubilization ratio, and a shift of the optimum salinity to a higher value.[65,66] The increasing pressure causes the molecules to move closer, increasing hydrophilic and lipophilic interaction due to more oil compressibility.[64] This proposed model is investigated for a range of increasing pressure (from 100 to 260 bar) at specific salinity conditions. The calculated results at 300 K and SDS of 0.21 mol L^{-1} are shown in Figure 13. The viscosity data indicate that there is a continuous increase in microemulsion viscosity across all salinity levels as pressure increases from 100 to 260 bar. This trend is distinct from the effect observed when the temperature increases. When pressure is increased from 100 to 260 bar, the viscosity of the microemulsion phase increases by 73.89% at a salinity of 0.11 mol L^{-1} and by 52.04% at a salinity of 0.35 mol L^{-1}. Increasing pressure tends to decrease the size of microemulsion droplets, leading to an increase in the interfacial area and potentially affecting the oil−water solubilization ratio. These smaller microemulsion droplets and the wider interfacial

https://doi.org/10.1021/acs.energyfuels.3c04902
Energy Fuels 2024, 38, 7746−7757

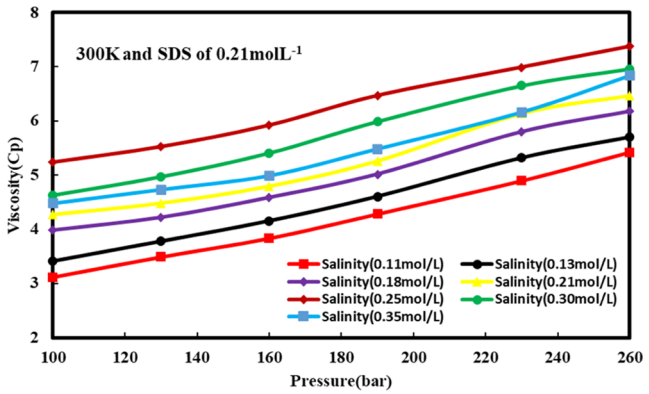

Figure 13. Pressure dependence of oil−water microemulsion viscosity at different salinities (300 K and SDS of 0.21 mol L^{-1}).

area between oil and water phases can exhibit higher viscosities due to increased interfacial interactions and surfactant layer thickness. This phenomenon can be illustrated by the experimental work of Skauge and Fotland,[65] where the authors examined the impact of pressure on the optimum solubilization ratio for the microemulsion system using the following equation:

$$S = \frac{V_o}{V_s} \tag{16}$$

where V_o and V_s are the volume fractions of oil and surfactant in the middle phase. The definition of water solubilization was considered analogous here. The authors found a change in the optimal salinity and solubilization ratio with increasing pressure. That means the viscous oil will see a greater change in optimal salinity conditions for increasing pressure.

4. CONCLUSIONS

We, for the first time, predicted the viscosity peaks or percolation threshold for the oil−brine−surfactant microemulsion phase at varying conditions. The microstructural changes in microemulsion phase viscosity are studied by using the MD simulation by examining an oil−water interface with varying concentrations of surfactant and salinity. The simulation work has been validated with previous experimental work in terms of IFT and viscosity. The results of this work are summarized as follows:

- The microemulsion phase viscosity is affected by SDS concentrations, with a sharp decrease in viscosity from 5.82 to 2.35 cP as the concentration increases from 0.18 to 0.24 mol L^{-1} and remains unchanged until 0.31 mol L^{-1}. The increasing SDS concentration (above 0.24 mol L^{-1}) increases the entanglement of the micelles, which hinders the movements of micelles in the microemulsion phase and hence increases the phase viscosity slightly.
- The hydrophilic−hydrophobic interaction of the SDS molecules and the increased salinity affects the viscosity peaks of the microemulsion phase by changing the solubility of SDS in the aqueous phase. The obtained viscosity curves are like a unique "M" shape and show two peaks as salinity increases due to the phase changes from brine to oil continuous phase. At high salinity conditions, the three phases (oil, surfactant, and brine) coexist, and the microemulsion phase exhibits shear-thinning behavior. On the contrary, when the salinity approaches the lower limit, the phase viscosity becomes extremely high and its shear-thinning behavior becomes more pronounced. Besides, the growing surfactant molecules in the middle phase cause the first peak of viscosity to move toward lower salinities and the second peak toward higher salinities, resulting in a deeper valley between the two peaks.
- Increasing temperature (from 300 to 450 K) reduces the phase viscosity continuously, with a decrease of 23.47% for a salinity of 0.11 mol L^{-1} and 26.69% for a salinity of 0.35 mol L^{-1}. The middle phase is surrounded by the release of excess oil until it reaches a specific temperature, after which it remains constant. On the contrary, as pressure increases from 100 to 260 bar, the viscosity of the microemulsion phase consistently increases for all salinity levels. The reason behind this is the decrement in the droplet size, which leads to an increase in interfacial area and potentially affects the oil−water solubilization ratio. The increasing pressure also resulted in a phase transition, a decrease in the optimum solubilization ratio, and a shift of the optimum salinity to a higher value.

Our extended work following this study will be generating sufficient data using a molecular dynamics simulation approach to develop a physics-based viscosity model to predict phase viscosity and percolation threshold of the oil−surfactant−brine microemulsion system as a function of salinity, surfactant concentration, temperature, and pressure for different types of surfactants and reservoir fluids.

AUTHOR INFORMATION

Corresponding Author

Akash Talapatra − *Department of Mining and Minerals Engineering, Virginia Tech, Blacksburg, Virginia 24061, United States;* orcid.org/0009-0008-0386-4468; Email: takash@vt.edu

Author

Bahareh Nojabaei − *Department of Mining and Minerals Engineering, Virginia Tech, Blacksburg, Virginia 24061, United States*

Complete contact information is available at: https://pubs.acs.org/10.1021/acs.energyfuels.3c04902

Author Contributions

A.T.: Methodology, investigation, validation, writing—original draft. B.N.: Conceptualization, supervision, writing, review, and rditing.

Notes

The authors declare no competing financial interest.

ACKNOWLEDGMENTS

This work was financially supported by the ACS PRF grant 2022. The authors also thank the ARC at Virginia Tech for the allocation of computing time on the TinkerCliffs cluster.

REFERENCES

(1) Wang, Y.; Chen, C. C. Enhanced Oil Production Owing to Sand Flow in Conventional and Heavy-Oil Reservoirs. *SPE Reserv. Eval. Eng.* **2001**, *4* (5), 366.

(2) Shi, L.; Liu, P.; Shen, D.; Liu, P.; Xi, C.; Zhang, Y. Improving Heavy Oil Recovery Using a Top-Driving, CO2-Assisted Hot-Water Flooding Method in Deep and Pressure-Depleted Reservoirs. *J. Pet. Sci. Eng.* **2019**, *173*, 922−931.

(3) Bashir, A.; Haddad, A. S.; Rafati, R. A Review of Fluid Displacement Mechanisms in Surfactant-Based Chemical Enhanced Oil Recovery Processes: Analyses of Key Influencing Factors. *Pet. Sci.* **2022**, *19*, 1211−1235.
(4) Bera, A.; Ojha, K.; Mandal, A.; Kumar, T. Interfacial Tension and Phase Behavior of Surfactant-Brine-Oil System. *Colloids Surf., A* **2011**, *383* (1−3), 114−119.
(5) Pal, S.; Mushtaq, M.; Banat, F.; Al Sumaiti, A. M. Review of Surfactant-Assisted Chemical Enhanced Oil Recovery for Carbonate Reservoirs: Challenges and Future Perspectives. *Pet. Sci.* **2018**, *15*, 77−102.
(6) Seng, L. Y.; Al-Shaikh, M.; Hascakir, B. Intermolecular Interaction between Heavy Crude Oils and Surfactants during Surfactant-Steam Flooding Process. *ACS Omega* **2020**, *5* (42), 27383−27392.
(7) Bera, A.; Mandal, A. Microemulsions: A Novel Approach to Enhanced Oil Recovery: A Review. *J. Pet. Explor. Prod. Technol.* **2015**, *5*, 255−268.
(8) Tagavifar, M.; Herath, S.; Weerasooriya, U. P.; Sepehrnoori, K.; Pope, G. Measurement of Microemulsion Viscosity and Its Implications for Chemical Enhanced Oil Recovery. *SPE J.* **2018**, *23*, 66−83.
(9) Jin, L.; Jamili, A.; Li, Z.; Lu, J.; Luo, H.; Ben Shiau, B. J.; Delshad, M.; Harwell, J. H. Physics Based HLD-NAC Phase Behavior Model for Surfactant/Crude Oil/Brine Systems. *J. Pet. Sci. Eng.* **2015**, *136*, 68−77.
(10) Acosta, E. J.; Bhakta, A. S. The HLD-NAC Model for Mixtures of Ionic and Nonionic Surfactants. *J. Surfactants Deterg.* **2009**, *12* (1), 7−19.
(11) Ghosh, S.; Johns, R. T. Dimensionless Equation of State to Predict Microemulsion Phase Behavior. *Langmuir* **2016**, *32* (35), 8969.
(12) Ghosh, S.; Johns, R. T. A Modified HLD-NAC Equation of State to Predict Alkali/Surfactant/Oil/Brine Phase Behavior. *SPE J.* **2018**, *23*, 550.
(13) Khorsandi, S.; Qiao, C.; Johns, R. T.; Torrealba, V. A. In *Simulation of Surfactant-Polymer Floods with a Novel Microemulsion Equation of State*, SPE − DOE Improved Oil Recovery Symposium Proceedings, 2016.
(14) *Microemulsions*; Robb, I. D., Ed.; Springer US: Boston, MA, 1982.
(15) Quemada, D.; Langevin, D.A Viscosity Model of Winsor Microemulsions. In *Surfactants in Solution*; Springer, 1989; p 123.
(16) Khurpade, P. D.; Nandi, S.; Jadhav, P. B.; Kshirsagar, L. K. In *CMG-Based Simulation Study of Water Flooding of Petroleum Reservoir*, Proceedings of the 7th International Conference on Advances in Energy Research, 2021.
(17) Khodaparast, P.; Johns, R. T. A Continuous and Predictive Viscosity Model Coupled to a Microemulsion Equation of State. *SPE J.* **2020**, *25* (3), 1070.
(18) Scriven, L. E. Equilibrium bicontinuous structure. *Nature* **1976**, *263*, 123−125.
(19) Peyrelasse, J.; Moha-Ouchane, M.; Boned, C. Viscosity and the Phenomenon of Percolation in Microemulsions. *Phys. Rev. A* **1988**, *38* (8), 4155.
(20) Lipgens, S.; Schübel, D.; Schlicht, L.; Spilgies, J. H.; Ilgenfritz, G.; Eastoe, J.; Heenan, R. K. Percolation in Nonionic Water-in-Oil-Microemulsion Systems: A Small Angle Neutron Scattering Study. *Langmuir* **1998**, *14* (5), 1041.
(21) Laurati, M.; Gambi, C. M. C.; Giordano, R.; Baglioni, P.; Teixeira, J. Small-Angle Neutron Scattering of Percolative Perfluoropolyether Water in Oil Microemulsions. *J. Phys. Chem. B* **2010**, *114* (11), 3855.
(22) Jeirani, Z.; Jan, B. M.; Ali, B. S.; See, C. H.; Saphanuchart, W. Pre-Prepared Microemulsion Flooding in Enhanced Oil Recovery: A Review. *Pet. Sci. Technol.* **2014**, *32* (2), 180.
(23) Kiran, S. K.; Acosta, E. J. Predicting the Morphology and Viscosity of Microemulsions Using the HLD-NAC Model. *Ind. Eng. Chem. Res.* **2010**, *49* (7), 3424−3432.
(24) Wen, B.; Sun, C.; Bai, B.; Gatapova, E. Y.; Kabov, O. A. Ionic Hydration-Induced Evolution of Decane-Water Interfacial Tension. *Phys. Chem. Chem. Phys.* **2017**, *19* (22), 14606−14614.
(25) Thompson, A. P.; Aktulga, H. M.; Berger, R.; Bolintineanu, D. S.; Brown, W. M.; Crozier, P. S.; in 't Veld, P. J.; Kohlmeyer, A.; Moore, S. G.; Nguyen, T. D.; Shan, R.; Stevens, M. J.; Tranchida, J.; Trott, C.; Plimpton, S. J. LAMMPS - a Flexible Simulation Tool for Particle-Based Materials Modeling at the Atomic, Meso, and Continuum Scales. *Comput. Phys. Commun.* **2022**, *271*, 108171.
(26) Siu, S. W. I.; Pluhackova, K.; Böckmann, R. A. Optimization of the OPLS-AA Force Field for Long Hydrocarbons. *J. Chem. Theory Comput.* **2012**, *8* (4), 1459.
(27) Lee, S. H. Temperature Dependence on Structure and Self-Diffusion of Water: A Molecular Dynamics Simulation Study Using SPC/E Model. *Bull. Korean Chem. Soc.* **2013**, *34* (12), 3800.
(28) Koziara, K. B.; Stroet, M.; Malde, A. K.; Mark, A. E. Testing and Validation of the Automated Topology Builder (ATB) Version 2.0: Prediction of Hydration Free Enthalpies. *J. Comput.-Aided Mol. Des.* **2014**, *28* (3), 221.
(29) White, A. *Intermolecular Potentials of Mixed Systems: Testing the Lorentz-Berthelot Mixing Rules with Ab Initio Calculations* Defence Science and Technology Organisation: Melbourne, Australia; 2000.
(30) Nik, N. S.; Abu Bakar, N. F.; Tengku Mohd, T. A.; Azizi, A. Molecular Dynamics Simulation on CO2 Foam System with Addition of SiO2 Nanoparticles at Various Sodium Dodecyl Sulfate (SDS) Concentrations and Elevated Temperatures for Enhanced Oil Recovery (EOR) Application. *Comput. Mater. Sci.* **2020**, *184*, No. 109937.
(31) Hess, B.; Bekker, H.; Berendsen, H. J. C.; Fraaije, J. G. E. M. LINCS: A Linear Constraint Solver for Molecular Simulations. *J. Comput. Chem.* **1997**, *18* (12), 1463.
(32) Stukowski, A. Visualization and Analysis of Atomistic Simulation Data with OVITO-the Open Visualization Tool. *Model. Simul. Mater. Sci. Eng.* **2010**, *18* (1), No. 015012.
(33) Zhao, J.; Yao, G.; Ramisetti, S. B.; Hammond, R. B.; Wen, D. Molecular Dynamics Simulation of the Salinity Effect on the N-Decane/Water/Vapor Interfacial Equilibrium. *Energy Fuels* **2018**, *32* (11), 11080−11092.
(34) Xuefen, Z.; Guiwu, L.; Xiaoming, W.; Hong, Y. Molecular Dynamics Investigation into the Adsorption of Oil-Water-Surfactant Mixture on Quartz. *Appl. Surf. Sci.* **2009**, *255* (13−14), 6493−6498.
(35) Choudhary, N.; Narayanan Nair, A. K.; Sun, S. Interfacial Behavior of the Decane + Brine + Surfactant System in the Presence of Carbon Dioxide, Methane, and Their Mixture. *Soft Matter* **2021**, *17* (46), 10545−10554.
(36) Green, M. S. Markoff Random Processes and the Statistical Mechanics of Time-Dependent Phenomena. II. Irreversible Processes in Fluids. *J. Chem. Phys.* **1954**, *22* (3), 398.
(37) Kubo, R. Statistical'Mechanical Theory of Irreversible Processes. I. General Theory and Simple Applications to Magnetic and Conduction Problems. *J. Phys. Soc. Jpn.* **1957**, *12* (6), 570.
(38) Helfand, E. Transport Coefficients from Dissipation in a Canonical Ensemble. *Phys. Rev.* **1960**, *119* (1), No. 1.
(39) Aminian, A.; ZareNezhad, B. Molecular Dynamics Simulations Study on the Shear Viscosity, Density, and Equilibrium Interfacial Tensions of CO2 + Brines and Brines + CO2 + n-Decane Systems. *J. Phys. Chem. B* **2021**, *125* (10), 2707−2718.
(40) Sedghi, M.; Piri, M.; Goual, L. Atomistic Molecular Dynamics Simulations of Crude Oil/Brine Displacement in Calcite Mesopores. *Langmuir* **2016**, *32* (14), 3375−3384.
(41) Rehfeld, S. J. Adsorption of Sodium Dodecyl Sulfate at Various Hydrocarbon-Water Interfaces. https://pubs.acs.org/sharingguidelines.
(42) DataPhysics Instruments GmbH. *Evaluating the Efficiency of Surfactants by Dynamic Interfacial Tension Measurements of Brine and Crude Oil*, 2000.
(43) Cui, X. L.; Pan, Y.; Hu, F. T.; Han, L.; Zhu, X. Y.; Zhang, L.; Zhou, Z. H.; Li, G.; Ma, G. Y.; Zhang, L. Dynamic Interfacial Tensions of Surfactant and Polymer Solutions Related to High-Temperature and High-Salinity Reservoir. *Molecules* **2023**, *28* (3), 1279.
(44) Yang, Y.; Pu, W. F. Low Interfacial Tension Emulsion Flooding under Harsh Reservoir Conditions: The Effect of Phase Inversion Behavior on Enhanced Oil Recovery. *J. Dispersion Sci. Technol.* **2020**, *41* (7), 1065−1074.

https://doi.org/10.1021/acs.energyfuels.3c04902
Energy Fuels 2024, 38, 7746−7757

(45) Spinler, E. A.; Zornes, D. R.; Tobola, D. P.; Moradi-Araghi, A. In *Enhancement of Oil Recovery Using a Low Concentration of Surfactant to Improve Spontaneous and Forced Imbibition in Chalk*, SPE/DOE Improved Oil Recovery Symposium, 2007.
(46) Dongqi, W.; Daiyin, Y.; Junda, W.; Yazhou, Z.; Chengli, Z. Influencing Factors and Microscopic Formation Mechanism of Phase Transitions of Microemulsion System. *J. Pet. Explor. Prod. Technol.* **2022**, *12* (10), 2735−2746.
(47) Gachuz-Muro, H. In *Effects of Brine on Crude Oil Viscosity at Different Temperature and Brine Composition-Heavy Oil/Water Interaction*, EAGE Annual Conference & Exhibition, 2013.
(48) Ahmed, S.; Elraies, K. A. Microemulsion in Enhanced Oil Recovery. In *Science and Technology Behind Nanoemulsions*; InTech, 2018.
(49) Wu, Z.; Yue, X.; Cheng, T.; Yu, J.; Yang, H. Effect of Viscosity and Interfacial Tension of Surfactant-Polymer Flooding on Oil Recovery in High-Temperature and High-Salinity Reservoirs. *J. Pet. Explor. Prod. Technol.* **2014**, *4* (1), 9−16.
(50) Georges, J.; Chen, J.-W.; Arnaud, N. Microemulsion Structure in the Lenticular Monophasic Areas of Brine/SDS/Pentanol/Dodecane or Hexane Systems: Electrochemical and Fluorescent Studies. *Colloid Polym. Sci.* **1987**, *265*, 45−51.
(51) Ivanova, A. A.; Phan, C.; Barifcani, A.; Iglauer, S.; Cheremisin, A. N. Effect of Nanoparticles on Viscosity and Interfacial Tension of Aqueous Surfactant Solutions at High Salinity and High Temperature. *J. Surfactants Deterg.* **2020**, *23* (2), 327−338.
(52) Nespolo, S. A.; Bevan, M. A.; Chan, D. Y. C.; Grieser, F.; Stevens, G. W. Hydrodynamic and Electrokinetic Properties of Decane Droplets in Aqueous Sodium Dodecyl Sulfate Solutions. *Langmuir* **2001**, *17* (23), 7210−7218.
(53) Shibaev, A. V.; Ospennikov, A. S.; Kuklin, A. I.; Arkharova, N. A.; Orekhov, A. S.; Philippova, O. E. Structure, Rheological and Responsive Properties of a New Mixed Viscoelastic Surfactant System. *Colloids Surf., A* **2020**, *586*, 124284.
(54) Victorov, A. I.; Molchanov, V. S.; Sorina, P. O.; Safonova, E. A.; Philippova, O. E. Modeling Micellar Growth and Branching in Mixtures of Zwitterionic with Ionic Surfactants. *Langmuir* **2022**, *38* (39), 11929.
(55) Gradzielski, M.; Duvail, M.; De Molina, P. M.; Simon, M.; Talmon, Y.; Zemb, T. Using Microemulsions: Formulation Based on Knowledge of Their Mesostructure. *Chem. Rev.* **2021**, *121*, 5671.
(56) Moulik, S. P.; Paul, B. K. Structure, Dynamics and Transport Properties of Micro Emulsions. *Adv. Colloid Interface Sci.* **1998**, *78* (2), 99.
(57) Negro, E.; Latsuzbaia, R.; De Vries, A. H.; Koper, G. J. M. Experimental and Molecular Dynamics Characterization of Dense Microemulsion Systems: Morphology, Conductivity and SAXS. *Soft Matter* **2014**, *10* (43), 8685−8697.
(58) Fu, Y.; Xiao, S.; Liu, S.; Chang, Y.; Ma, R.; Zhang, Z.; He, J. Atomistic Insights into the Droplet Size Evolution during Self-Microemulsification. *Langmuir* **2022**, *38* (10), 3129−3138.
(59) Ho, T. M.; Razzaghi, A.; Ramachandran, A.; Mikkonen, K. S. Emulsion Characterization via Microfluidic Devices: A Review on Interfacial Tension and Stability to Coalescence. *Adv. Colloid Interface Sci.* **2022**, *299*, No. 102541.
(60) Li, R.; Wang, Z.; Gu, X.; Chen, C.; Zhang, Y.; Hu, D. Study on the Assembly Structure Variation of Cetyltrimethylammonium Bromide on the Surface of Gold Nanoparticles. *ACS Omega* **2020**, *5*, 4943−4952.
(61) Ma, J.; Song, X.; Luo, J.; Zhao, T.; Yu, H.; Peng, B.; Zhao, S. Molecular Dynamics Simulation Insight into Interfacial Stability and Fluidity Properties of Microemulsions. *Langmuir* **2019**, *35* (42), 13636.
(62) *Surfactants in Solution*; Mittal, K. L., Ed.; Springer: US, 1986.
(63) Bera, A.; Kumar, S.; Mandal, A. Temperature-Dependent Phase Behavior, Particle Size, and Conductivity of Middle-Phase Microemulsions Stabilized by Ethoxylated Nonionic Surfactants. *J. Chem. Eng. Data* **2012**, *57* (12), 3617−3623.
(64) Johns, R. T.; Pope, G. A.; Lake, L. W.; Delshad, M.; Dindoruk, B. *Effect of Pressure and Methane on Microemulsion Phase Behavior and Its Impact on Surfactant* Polymer Flood Oil Recovery Committee; 2010.
(65) Skauge, A.; Fotland, P. Effect of Pressure and Temperature on the Phase Behavior of Microemulsions. *SPE Reserv. Eng.* **1990**, *5*, 601−608.
(66) Zhao, G.; Khin, C. C.; Chen, S. B.; Chen, B. H. Nonionic Surfactant and Temperature Effects on the Viscosity of Hydrophobically Modified Hydroxyethyl Cellulose Solutions. *J. Phys. Chem. B* **2005**, *109* (29), 14198−14204.

https://doi.org/10.1021/acs.energyfuels.3c04902
Energy Fuels 2024, 38, 7746−7757